Design of a Porous Bluff-Body Disc on Improving the Gas-Mixing Efficiency

Shun-Chang Yen, You-Lun Peng, and Kuo-Ching San

Abstract—**A bluff body with multiple holes was designed to transform the axial momentum into radial and tangential momentum for increasing the swirl number (S). A numerical study of bluff-body structure with multiple holes was performed using ANSYS Fluent computational fluid dynamics (CFD) analysis. The effects of hole number and jet inclination angles were considered using a fixed gas flow rate and a non-reactive gas. The concentration distribution behind the mixing of central carbon-dioxide (CO_2) jet and annular air jet was utilized to analyze the mixing efficiency. Three bluff bodies with differing hole numbers (H = 3, 6, and 12), three different jet inclination angles (θ = 30°, 45°, and 90°) were designed for the analysis. The Reynolds normal stress increases with the inclination angle. The Reynolds shear stress, averaged turbulence intensity and a/veraged swirl number decrease with the inclination angle. For the unsymmetrical hole configuration (i.e., H = 3), the streamline patterns shows a unsymmetrical flow field. The highest mixing efficiency (i.e., the lowest integral gas fraction of CO_2) occurs at H = 3. Furthermore, the highest swirl number coincident the strongest effect on the mass fraction of CO_2. The unsymmetrical hole arrangement induces a high swirled flow behind the porous disk.**

Index Terms—**Bluff body with multiple holes; Computational fluid dynamics (CFD); Swirl-jet flow; Mixing efficiency**

I. INTRODUCTION

THE spray nozzles have been widely utilized in the daily life, such as the sprinkler, gas burner and fuel atomizer. The nozzle area, nozzle-matrix spacing and central-to-annular jet ratio were adjusted to intensify the combustion intensity. The improvement of combustion efficiency can diminish the energy dissipation and exhaust emission. The swirl flow was utilized to increase the mixing rate between the fuel and air jets. The swirl mechanism changes the axial-flow momentum to tangential flow. The increased tangential velocity intensified the swirl number in the flow field. In addition, the increased swirl flow generated a inverse pressure gradient in the axial direction and the vortex break-down occurred at a specific critical value of swirl number. The increased swirl number improved the flow mixing. Specifically, the fuel-to-air mixing was improved efficiently and the combustion stability.

A high adverse pressure gradient occurs in front of the bluff bodies when a uniform and steady flow moved pass the bluff bodies, and then a low-pressure zone occurs behind the bluff bodies. Furthermore, the separation occurs near the leading edge of bluff bodies and generates the separated shear layer. In the downstream, the interaction between the shear layer generates a large-scale recirculation. In the previous studies, Strouhal [1] experimentally investigated the vortex shedding behind a circular cylinder. He found that the Strouhal number (i.e., a dimensionless parameter defined as fD/U) approaches a constant at a specific range of Reynolds numbers. Von Karman [2] studied the vortex strip generated behind a circular cylinder and presented a quantification description using this shedding regularity. In the experimental apparatus, Huang and Tsai [3, 4] utilized the laser Doppler Velocimetry (LDV) and smoke-wire visualization to investigate the flow structures using different blockage ratios and swirl numbers. They found that the bluff-body effect is significant when the blockage ratio is greater than 0.1. Al-Abdeli [5] used the LDV to investigate the unconfined flow behaviors behind a circular disc. He found that the recirculation zone correlates with the swirl number and the radial diffusion depends on the axial velocity and swirl number. In the practical applications, Huang and Yen [6] utilized the swirl flow perturbed using an airfoil van pack. They defined three flame modes: weak swirling flame, lifted flame and turbulent reattached flame. San and Hsu [7] utilized a rifled nozzle to increase the mixing efficiency between the central fuel and annular air jets. They classified the flame patterns as jet, flickering and turbulent flames. San *et al.* utilized a rifled cone to increase the mixing rate between the central CO_2-jet and the annular air-jet. Three cold-flow structures were defined: jet flow, single bubble and dual bubble. Yen and Shih [8] utilized a spiral-grooved cone to intensify the bluff-body effect and increase the turbulence intensity. They found these grooves can increase the mixing efficiency and combustion intensity; and however decrease the flame length.

Many studies utilized the numerical scheme/software to investigate the bluff-body flow behaviors. Dally *et al.* [9] simulated the flow fields and mixing fields utilizing the standard models and found that two vortex occurred in the recirculation zone. They also found that the modified k-ε scheme and Reynolds stress turbulent flow model can predict more accurate position of recirculation zone. Wouters *et al.* [10] also utilized the k-ε Reynolds stress model to analyze the effects of geometrical shape on the gas mixing ratio. Wegner *et al.* [11] utilized the U-RANS (unsteady Reynolds averaged Navier-Stokes) to simulate a non-premixed swirl burner. The numerical results were compared with the experimental and

LES (large eddy simulation) results. The comparison results show that the U-RANS algorithm can quantitatively calculated the processing vortex core (PVC). Zhang, *et al.* [12] utilized the LES algorithm to study the coherent structures behind a bluff body. They found three vortex structures using the Q-function visualization. These vortex structures are cylindrical shell structure in the outer shear layer, ring structure and hairpin-like structures in the inner shear layer. Jenny *et al.* [13] utilized three different probability density functions (PDF) to study a constant-density bluff-body stabilized flow. The three algorithms included a standalone particle-mesh method and two hybrid algorithms. Their results show that the three numerical algorithms are satisfied with the experimental data.

The mixing mechanism is a critical issue in combustion field. This issue includes the time-shortening and space-narrowing of fuel and air. This study combined a bluff-body disc and hole structures to adjust the air jet near the nozzle exit. The spiral hole structures drove the air flowed in the tangential direction and generated the swirl flow. The bluff bodies were frequently utilized in the combustors to increase the flame detention time and intensify the mixing between fuel and air. Namely, the bluff body is a passive device utilized to improve the combustion intensity. This investigation utilized the numerical simulation to study the turbulent flow field behind the three-dimensional multi-hole bluff body. The investigation parameters included the hole geometry, hole numbers and air-jet incidence angle.

II. MATHEMATICAL MODEL

Many intricate fluid dynamic topics have been solved using the commercial software programs based on the finite volume algorithm. This investigation utilized the software package – ANSYS Fluent 15.0 – to analyze the flow behaviors behind the porous bluff-body disk.
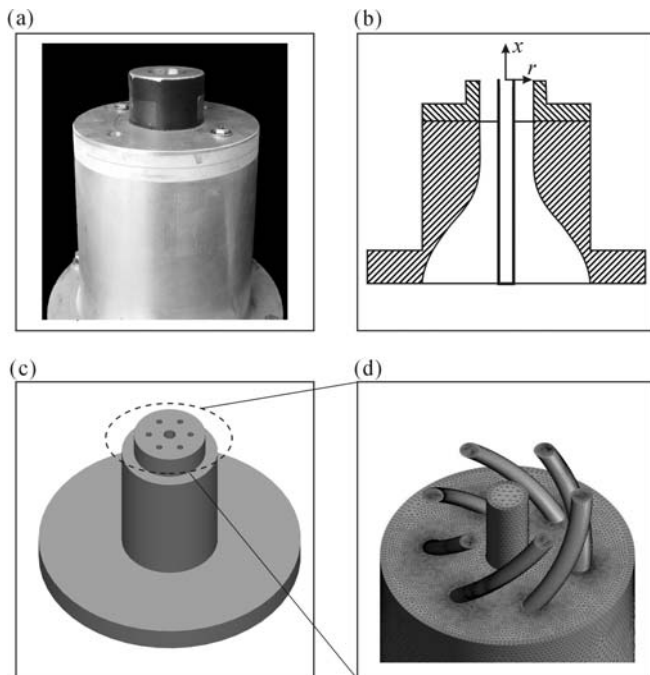

Fig. 1. Design of pure-jet nozzle. (a) Pure-jet nozzle; (b) Sectional view, (c) Numerical model, and (d) Numerical model of hole structure.

A. Hypotheses

In the nozzle, the flow field is very complicated. Therefore, the simplified model must be presented to lower the computation loading. These hypotheses suggested in this investigation includes (1) three dimensional unsteady flow field, (2) turbulent flow field, (3) Newtonian flow, (4) no slip boundary condition, (5) Cartesian coordinate system, (6) neglected gravity effect, and (7) constant room temperature.

B. Governing Equations

The vector forms of three-dimensional continuity equation (Eq. 1) and Navier-Stokes equations (Eq. 2) are listed as follows.

$$\frac{\partial \rho}{\partial t} + \nabla(\rho U) = 0 \tag{1}$$

$$\frac{\partial(\rho U)}{\partial t} + \nabla \cdot (\rho U \otimes U + \mathrm{p}I) = \nabla \cdot \tau + \rho g. \tag{2}$$

Turbulent Models. Kolmogorov (1942) suggested the first and complete turbulent model. In this study, a standard *k-ε* model was utilized and assumed that the turbulent flow field was fully developed. The standard turbulent *k-ε* model is listed as follows (Eq. 3).

$$\frac{\partial}{\partial t}(\rho k) + \frac{\partial}{\partial x_1}(\rho k u_i) = \frac{\partial}{\partial x_i} \cdot$$

$$\left[\left(\mu + \frac{\mu_t}{\sigma_k} \right) \frac{\partial k}{\partial x_i} + G_k + G_b - \rho \varepsilon \right]. \tag{3}$$
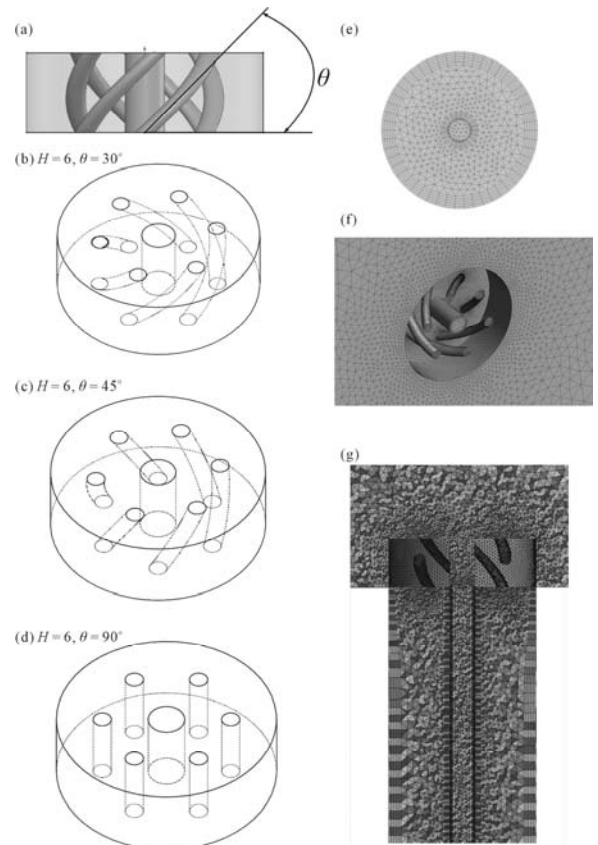

Fig. 2. Meshgrid graph.

where G_k presents the turbulent kinetic energy caused from the average velocity, G_b is the turbulent kinetic energy caused from the buoyant force, and ε represents the effect of compressible turbulent pulse expansion on total dissipation rate.

C. Model Design

Figure 1(a) shows the physical pure-jet nozzle [6]. The inner fuel jet and annular airflow compose the non-premixed flame mechanism. Figure 1(b) shows the coordinate system utilized in this study, where x indicated the axial direction and r represents the radial axis. The inner diameter of central jet (D_i) is 5 mm and the outer diameter of annular jet (D_o) is 30 mm. Figure 1(c) shows the model and annular hole design utilized in this numerical study where the diameter of annular air hole (D_h) is 2.5 mm. Figure 1(d) shows the computation mesh characterized the spiral hole structures. In this numerical calculation, the hole numbers (H) were chosen as 3, 6, 12 and the inclination angle (θ) of this spiral air hole was set at 45, 60 and 90 degree.

The open boundary condition was set at the boundary of calculation domain which is 5 times of the outer diameter of annular airflow (i.e., D_i). In the axial direction, the calculation domain is 12 times of the outer-flow diameter for transforming the flow to fully developed. At the inlet, the boundary condition was set at constant velocity of 0.2 m/s. The boundary condition for the open boundary was set at outlet pressure of 101,325 Pa (i.e., 1 atm).
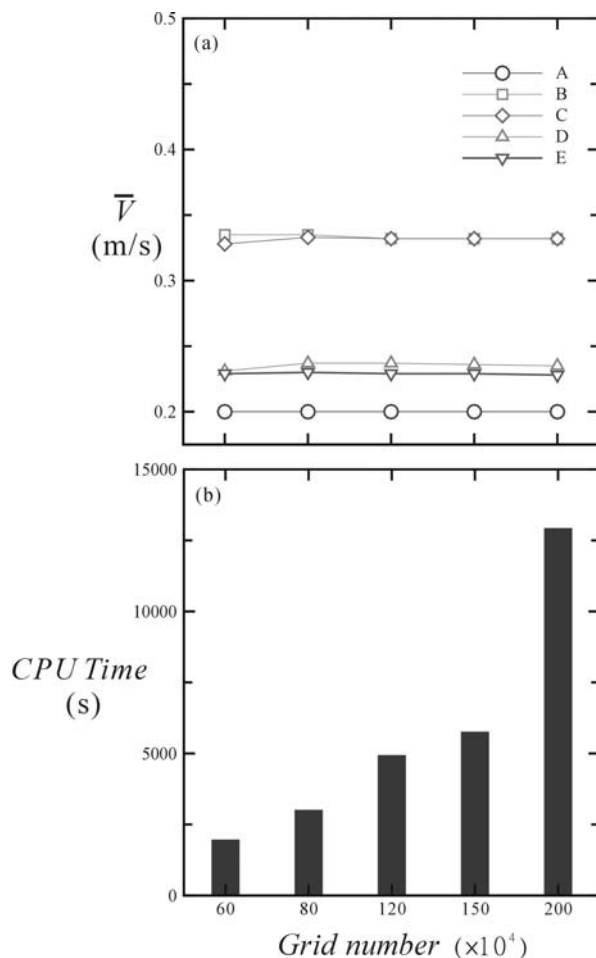
This study utilized the tetrahedral mesh to analyze the flow behaviors behind the porous bluff body. The boundary mesh was utilized near the calculation boundary. This investigation utilized the ANSYS Meshing to generate the calculation mesh. The designed model was input into ANSYS to mesh the flow field. Figure 2(a) shows the spiral hole structure and reveals the definition of inclination angle. Figure 2(b)-2(d) show the perspective view for $H = 6$ at $\theta = 30°$, 45° and 90°, respectively. Figure 2(e) show the top view of the mesh structure for the flow field. Figure 2(f) shows the mesh structure near the jet exit. In this calculation domain, there is a significant change of velocity and pressure. Therefore, the mesh density was intensified to increase the computation accuracy. Figure 2(g) shows the side view of the whole computation domain. The airflow was driven from the bottom, passing through the hole structures, and then flew into the free space.

D. Element and CPU time

This investigation focused on the flow velocity field and the distribution of mixing concentration. In the computation domain, five points of A – E (shown in the inset of Fig. 3(a)) were chosen to measure the flow properties. The effect of grid numbers on the flow velocity is shown in Fig. 3(a). Figure 3(a) shows that the flow velocity approaches stably when the grid number is larger than 1.2×10^6.
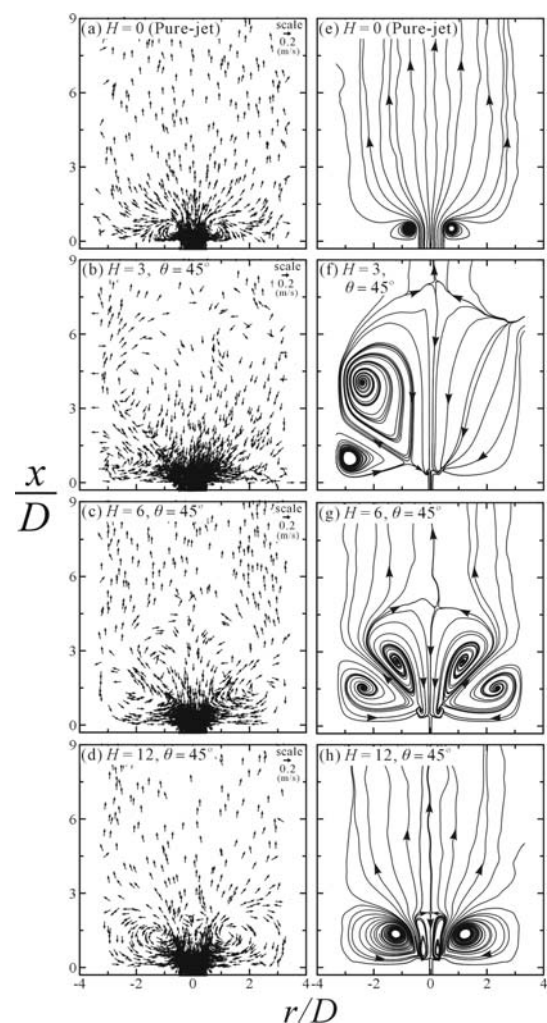

Fig. 3. (a) Average velocity vs. Grid number, and (b) CPU time vs. Grid number.

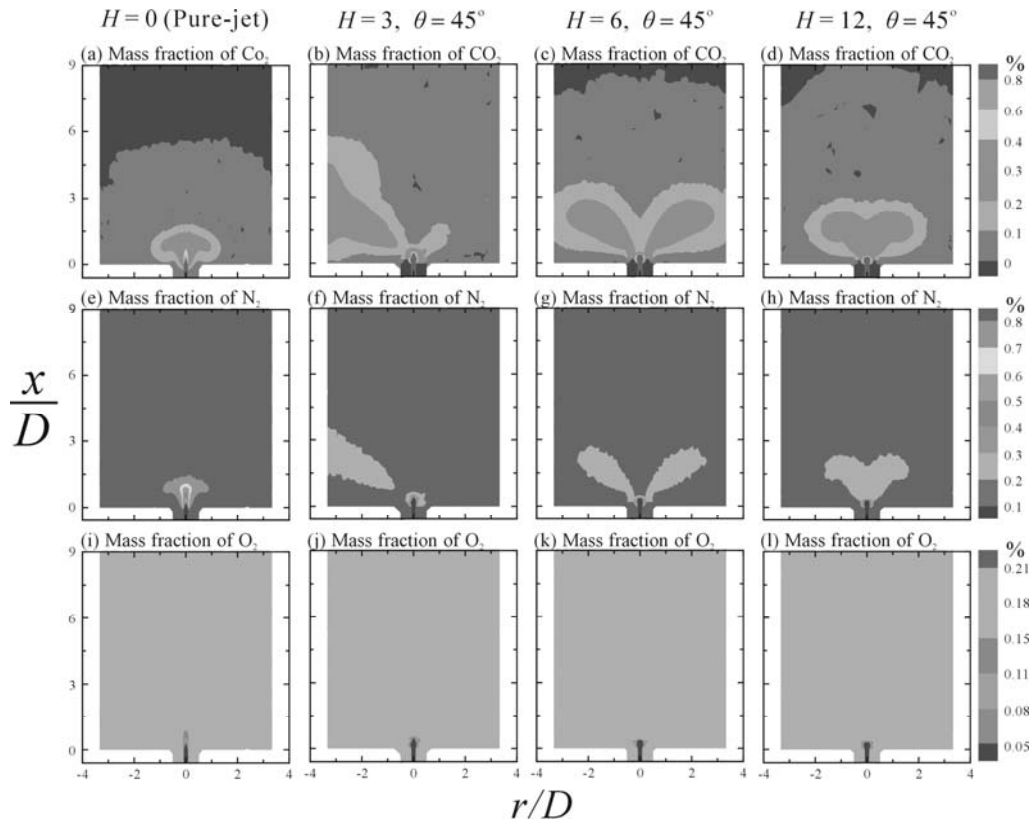Fig. 4. (a) – (d) Velocity vectors and (e) – (h) Stream lines.

Fig. 5. Mass fraction of CO_2, N_2 and O_2.

Figure 3(b) shows the relation of CPU time and grid numbers. For considering the factors of CPU time and calculation stabilization, this study utilized the grid number of 1.5×10^6 to numerically analyze the whole flow field.

III. RESULTS AND DISCUSSION

A. Velocity vectors and Stream lines

Figure 4 shows the velocity vectors (Figs. 4(a)-(d)) and stream lines (Fig. 4(e)-(h)) behind a pure jet and different hole-numbered disc. The test conditions were: (1) central-jet velocity $(u_c) = 0.2$ m/s; (2) annular-jet velocity $u_a = 0.2$ m/s; (3) hole number $(H) = 0$ (i.e., pure jet), 3, 6, 12; and (4) inclination angle $(\theta) = 45°$.

Figures 4(a) and 4(e) show that two recirculations appear near the nozzle exit due to the entrainment effect. With the effects of holes and inclination angel, Figs. 4(b) and 4(f) show that two recirculations occur behind the left side of 3-hole disc. The un-symmetric hole arrangement caused the un-symmetric flow structures. In addition, Fig. 4(s) shows a four-way saddle point occurring at $x/D = 7.7$. Figures 4(c) and 4(g) show that six recirculations (three pairs) occurs behind the six-hole disc. Figure 4(g) shows a four-way saddle point appear at $x/D = 4.5$. Figures 4(d) and 4(h) show four symmetric recirculations (two pairs) occurs behind a 12-hole disc. The four-way saddle point occurs at $x/D = 2.1$. The distance between the four-way saddle point and nozzle exit decreases with the increase of hole number due to the intensification of turbulence intensity. Namely, the spiral hole structure drove the axial flow to tangential flow and improve the interaction between central and annular flows.

B. Concentration Distributions

Figure 5 shows the distributions of mass fraction for CO_2, N_2 and O_2. For the pure jet nozzle, the CO_2 is accumulated near the jet exit. The CO_2 was lifted from the jet exit as the CO_2 exhaled from the holes. Figure 5(d) shows the un-symmetric arrangement of hole configuration. For the mass fraction of N_2 and O_2, very low fraction of N_2 and O_2 were entrained in the central zone near the jet exit. The mass fraction of N_2 and O_2 in the downstream agrees with the standard atmospheric condition.

IV. CONCLUSIONS

Bluff-body discs drilled with multiple holes were examined to increase the mixing efficiency in the cold flow field. This design was numerically performed using the commercial ANSYS Fluent software. The test condition setting a fixed air flow and a non-reactive CO_2 gas and changing the number of holes, and jet inclination angles. The swirl number (S) and turbulence intensity $(T.I.)$ were introduced to indicted the effects of these factors on the CO_2 distribution. The following conclusions were summarized from the calculated results.

1) For a pure jet (i.e., $H = 0$), $H = 6$ and $H = 12$ porous discs, the streamline patterns show the symmetrical configurations. For a $H = 3$ holed disc show a unsymmetrical streamline pattern.

2) For the un-symmetric arrangement of hole configuration (i.e., $H = 3$), very low fraction of N_2 and O_2 were entrained in the central zone near the jet exit.

3) The highest mixing efficiency occur at $H = 3$ (i.e., the

lowest integral gas fraction of CO_2 occurring at $H = 3$) due to the unsymmetrical hole arrangement.

4) For a $H = 3$ disk, the highest swirl number coincident the strongest effect on the mass fraction of CO_2. The unsymmetrical hole arrangement induces a high swirled flow behind the porous disk.

REFERENCES

[1] V. Strouhal, "Ueber eine besondere art der tonerregung (On an unusual sort of sound excitation)," *Annalen der Physik und Chemie*, vol. 5, no. 10, 1878, pp. 216-251.

[2] T. Von Kármán, *Aerodynamics*. New York: McGraw-Hill, 1963.

[3] R. F. Huang and F. C. Tsai, "Observations of swirling flows behind circular discs," *AIAA J.*, vol. 39, 2001, pp. 1106-1112.

[4] F. C. Tsai, "Flow structure and mixing characteristics of swirling wakes," Ph.D. dissertation, Dept. Mech. Eng., National Taiwan University of Science and Technology, Taipei, Taiwan, 2001.

[5] Y. M. Al-Abdeli and A. R. Masri, "Recirculation and flowfield regimes of unconfined non-reacting swirling flows," *Experimental Thermal and Fluid*, vol. 27, 2003, pp. 655-665.

[6] R. F. Huang and S. C. Yen, "Aerodynamic characteristics and thermal structure of nonpremixed reacting swirling wakes at low Reynolds numbers," Combustion and Flame, vol. 155, 2008, pp. 539-556.

[7] K. C. San and H. J. Hsu, "Characteristics of flow and flame behavior behind rifled/unrifled nozzles," *ASME Journal of Engineering for Gas Turbines and Power*, vol. 131, 2009, pp. 051501.

[8] S. C. Yen and C. L. Shih, "Improving combustion intensity and modulating flame behaviors using helical-grooved cones," Journal of Mechanics, vol. 29, 2013, pp. 273-280.

[9] B. B. Dally, A. R. Masri, R. S. Barlow, and G. J. Fiechtner, "Instantaneous and mean compositional structure of bluff-body stabilized nonpremixed flames," Combustion and Flame. vol. 114, 1998, pp. 119-148.

[10] H. A. Wouters, P. A. Nooren, T. W. J. Peeters, and D. Roekaerts, "Simulation of a bluff-bodystabilized diffusion flame using second-moment closure and Monte Carlo methods," *Symposium on Combustion*, vol. 26, no. 1, 1996, pp. 177-185.

[11] B. Wegner, A. Maltsev, C. Schneider, A. Sadiki, A. Dreizler, and J. Janicka, "Assessment of unsteady RANS in predicting swirl flow instability based on LES and experiments," *International Journal of Heat and Fluid Flow*, vol. 25, 2004, pp. 528-536.

[12] P. Zhang, C. Han, and Y. Chen, "Large eddy simulation of flows after a bluff body: Coherent structures and mixing properties," *Journal of Fluids and Structures*, vol. 42, 2013, pp. 1-12.

[13] P. Jenny, M. Muradoglu, K. Liub, S. B. Pope, and D. A. Caughey, "PDF simulations of a bluff-body stabilized flow," *Journal of Computational Physics*, vol. 169, 2001, pp. 1-23.